Author version of accepted manuscript published in Journal of Neuroscience Methods, available online 17/07/2020
https://doi.org/10.1016/j.jneumeth.2020.108870

Regional segmentation strategy for DTI analysis of human corpus callosum indicates motor function deficit in mild cognitive impairment

Surya Rajan[1], Julia Brettschneider[2] and Joanna F Collingwood[1*], for the Alzheimer's Disease Neuroimaging Initiative[+]

Addresses:
[1]School of Engineering, University of Warwick, Coventry, UK
[2]Department of Statistics, University of Warwick, Coventry, UK

[*]Corresponding author details:
Joanna F Collingwood,
School of Engineering,
University of Warwick,
Coventry, United Kingdom
CV4 7AL
Email: J.F.Collingwood@warwick.ac.uk

[+]Data used in preparation of this article were obtained from the Alzheimer's Disease Neuroimaging Initiative (ADNI) database (adni.loni.usc.edu). As such, the investigators within the ADNI contributed to the design and implementation of ADNI and/or provided data but did not participate in analysis or writing of this report. A complete listing of ADNI investigators can be found at: http:// adni.loni.usc.edu/wpcontent/ uploads/ how_to_apply/ ADNI_Acknowledgement_List.pdf

Keywords
Corpus callosum, diffusion tensor imaging, ageing, mild cognitive impairment, motor impairment

Abstract

Background: The corpus callosum is the largest white matter tract in the human brain, involved in inter-hemispheric transfer and integration of lateralised visual, sensory-motor, language, and cognitive information. Microstructural alterations are implicated in ageing as well as various neurological conditions.

New Method: Cross-sectional diffusion-weighted images of 107 healthy adults were used to create a linear regression model of the ageing corpus callosum and its sub-regions to evaluate the impact of analysis by sub-region, and to test for deviations from healthy ageing parameters in 28 subjects with mild cognitive impairment (MCI). Alterations in diffusion properties including fractional anisotropy, mean, radial and axial diffusivities were investigated as a function of age.

Results: Changes in DTI parameters showed age-dependent regional differences, likely arising from axonal diameter variation across cross-sectional regions of interest in the corpus callosum. Patterns suggestive of degeneration with healthy ageing were observed in all regions. Diffusion parameters in sub-regions projecting to pre-motor, primary, and supplementary motor areas of the brain differed for MCI versus healthy controls, and MCI subjects were more likely than healthy controls to experience a reduction in motor skills.

Comparison with Existing Methods: Statistical analyses of the corpus callosum by five manually-defined sub-regions, instead of a single manually-defined region of interest, revealed region-specific changes in microstructure in healthy ageing and MCI, and accounted for clinically-evaluated differences in motor skills between cohorts.

Conclusion: This method will support future studies of corpus callosum, enabling identification and measurement of white matter changes that are undetectable with the single ROI approach.

1. Introduction

The topology of the human brain is constantly changing from birth, plateauing in adulthood and degenerating in later life. Both grey matter and white matter tissues in the brain are susceptible to ageing, with observations in post-mortem studies of healthy human brains of more severe age-related changes in white matter than in grey matter (Marner et al., 2003; Piguet et al., 2009). The corpus callosum is the largest white matter tract in the human brain, with more than 300 million fibres interconnecting the two cerebral hemispheres. Recent technological advances have found fibres of the corpus callosum projecting into prefrontal, pre-motor, supplementary and primary motor, and sensory areas of the brain (Hofer and Frahm, 2006), and involved in inter-hemispheric transfer and integration of lateralised visual, sensory-motor, language and cognitive information (van der Knaap and van der Ham, 2011). Corpus callosum anatomy has been divided into sub-regions based on geometry (Clarke and Zaidel, 1994; Witelson, 1989), connectivity (Hofer and Frahm, 2006), and statistically derived cohesiveness (Denenberg et al., 1991; Peters et al., 2002). Studies on effects of age, sex and handedness in the healthy brain have reported differences in these properties in the corpus callosum by sub-region (Peters et al., 2002; Prendergast et al., 2015; Reuter-Lorenz and Stanczak, 2000; Sullivan et al., 2001b; Witelson, 1989).

Post-mortem studies have linked altered properties of the corpus callosum to normal ageing (Hou and Pakkenberg, 2012) as well as neurological disorders including schizophrenia (Woodruff et al., 1995), multiple sclerosis (Evangelou et al., 2000), Huntington's disease and progressive supranuclear palsy (Mann et al., 1993). Recent magnetic resonance imaging (MRI) studies have strengthened these conclusions with evidence of atrophy (Goldman et al., 2017; Granberg et al., 2015; Lee et al., 2016; Wang et al., 2015a), morphological changes (Ardekani

et al., 2014; Pardoe et al., 2015; Wolff et al., 2015), and demyelination in the human corpus callosum (Decker et al., 2018; Køster et al., 2018) and mouse models (Xiu et al., 2015). Diffusion tensor magnetic resonance imaging (DT-MRI or DTI) has also been applied to study the corpus callosum. DTI is an advanced technique that is used to image the diffusion properties of water molecules in tissue, providing a means to interpret the presence or absence of barriers to this diffusion (Le Bihan et al., 2001). DTI has been previously used to study the microstructural properties of the corpus callosum in healthy ageing and various neurological disorders (Hasan et al., 2005; Shahab et al., 2018; Sullivan and Pfefferbaum, 2003).

The corpus callosum is reportedly the white matter structure most affected by age (Sala et al., 2012), with some studies also revealing differences in the extent to which its sub-regions are affected (Ota et al., 2006). These variations between the sub-regions have been suggested as indicative of the differing effects of age in the corresponding parts of the brain they project to (Lebel et al., 2010; Ota et al., 2006). However, there are conflicting study results in the literature with some indicating a larger effect of age in the anterior corpus callosum than in the posterior (Hasan et al., 2005; Lebel et al., 2010; Ota et al., 2006; Sullivan et al., 2001a, 2001b), and a few suggesting the opposite (Bennett et al., 2017). MRI and DTI studies of the corpus callosum have also been carried out for various neurological disorders including mild cognitive impairment (MCI) and Alzheimer's disease (AD) (Ardekani et al., 2014; Lee et al., 2016; Wang et al., 2015b). Results of these studies indicate degeneration of the corpus callosum in disease that exceeds changes arising from healthy ageing.

The corpus callosum incorporates a heterogeneous bundle of fibres connecting the hemispheres of the brain. Different segments of this fibre bundle have been observed to be of different sizes or diameters, likely depending on the region of the brain they project to (Aboitiz et al., 1992). This may have an impact on the quantitative parameters measured *in vivo*, particularly in DTI. In previous DTI investigations of the corpus callosum in healthy ageing and disease, it has been treated as a single region of interest (ROI), and/or by sub-region (Ma et al., 2009, Bennett et al., 2017, Feng et al., 2018, Ota et al., 2006, Lebel et al., 2010). While a single ROI approach is easier to implement, the heterogeneity of the corpus callosum may be better represented through a region-wise analysis. This, in turn, may be influenced by the choice of scheme used to define the sub-regions. Here, we investigated DTI properties of the corpus callosum as a function of age and tested for cohort differences between ageing healthy controls (HC) and individuals with MCI, examining how this is influenced by segmenting the corpus callosum as a single ROI and by sub-region. Strategies for segmentation of the corpus callosum were explored. The data available to this study were acquired in the axial plane, but the corpus callosum is better delineated in the sagittal plane, so at the outset comparisons were made between atlas-based and manual delineation of the corpus callosum to determine the most appropriate strategy for this study. Having selected a manual delineation approach, the Hofer and Frahm scheme (segmenting in the sagittal plane to create pre-defined fractions), was used to divide the corpus callosum into five sub-regions for analysis (Hofer and Frahm, 2006).

2. Materials and Methods

Data used in this study were obtained from the Alzheimer's Disease Neuroimaging Initiative (ADNI) database (http://adni.loni.usc.edu). ADNI was launched in 2003 as a public-private

partnership, led by Principal Investigator Michael W. Weiner, MD. The primary goal of ADNI has been to test whether serial MRI, positron emission tomography, other biological markers, and clinical and neuropsychological assessments can be combined to measure the progression of MCI and early AD. ADNI consists of a series of multi-site data acquisition studies, with ADNI-1, ADNI-2, and ADNI-GO completed to date; ADNI-3 is ongoing. This study used data from ADNI-3, in order to utilize DTI data acquired at higher spatial resolution than in the previous ADNI studies. The primary inclusion criterion was that the image data were acquired with a set of fully-matched scan parameters. Prior studies confirm the importance of ensuring a consistent set of acquisition scan parameters to avoid introducing experimental uncertainty into the quantitative results, where their selection reportedly affects diffusion tensor estimation in DTI (Landman et al., 2007; Zavaliangos-Petropulu et al., 2019, Zhu et al., 2009). Application of this criterion to the full cohort in ADNI-3 produced a choice of three study cohorts (Siemens, GE, or Philips), and the largest of these at the time of analysis (Siemens) was selected, providing 140 subjects (107 HC, 28 MCI, 5 AD). All these HC and MCI subjects were included in the present study. Although the sample sizes for HC and MCI differed, this was carefully considered and accommodated for in the choice of statistical methods for comparison between the groups. The 5 AD cases were excluded because power calculations to determine study group size, based on prior-published ADNI-2 data, indicated that the AD group was too small to include for comparison with the HC and MCI.

The scan sequence details of images included in this study are: field strength = 3 T, echo time (TE) = 56 ms, repetition time (TR) = 7200 ms, b = 0, 1000 s/mm^2, number of diffusion weighted images = 48, number of non-diffusion weighted images = 7, voxel size = 2 mm x 2 mm x 2 mm and approximate scan time = 7 mins 30 s.

The ADNI-3 subject images selected for use in this study were collected at the baseline visit for each participant. Ideally, longitudinal data from individuals would be used to analyse changes in DTI parameters as a function of age. In practice, a preliminary analysis (using the lower-spatial-resolution longitudinal data sets from ADNI-2 (Supplementary Figure S1) confirmed an insufficient number of participants in the ADNI-3 study cohort to support a longitudinal analysis. Instead, a cross-sectional analysis of the data from ADNI-3 was performed; this had the advantage of enabling inclusion of all HC and MCI subjects imaged using Siemens scanners during ADNI-3.

Gender has been reported to be a significant risk factor for MCI and AD, with the longitudinal rate of cognitive decline in MCI observed to be greater in women than in men (Laws et al., 2018, Lin et al., 2015). Gender-dependence of the patterns of change in DTI parameters of the white matter have also been observed (Kanaan et al., 2012); however, this finding is contradicted by others where no gender differences were observed (Inano et al., 2011). This apparent difference may be accounted for by factors other than gender dominating the white matter changes (de Schotten et al., 2011). For this reason, differences in DTI parameters as a function of gender were specifically tested for in the ADNI-3 cohorts studied here.

To understand if gender influenced DTI parameters with ageing, HC_{sub} (74 age- and gender-matched healthy subjects (37 F; 37 M)) was created as a subset of the main HC study group. Subject demographics are summarised in Table 1. The rationale for creating HC_{sub} was to test, using multiple regression, whether the DTI parameters were influenced by gender, and thereby to determine whether the main cohort HC or the subset HC_{sub} was most appropriate for use in the study of the relationship between DTI parameters and ageing.

Table 1: Age and gender distribution of subjects in the main healthy control (HC) and mild cognitive impairment (MCI) cohorts, and the gender- and age-matched HC subgroup (HC_{sub}) as a subset of the HC cohort; M: male, F: female.

Age range (years)	**Healthy controls**			**Mild cognitive impairment**	
	Cohort	**M**	**F**	**M**	**F**
55-60	HC	-	1	-	2
	HC_{sub}	-	-		
61-65	HC	5	8	1	-
	HC_{sub}	5	5		
66-70	HC	7	24	2	1
	HC_{sub}	7	7		
71-75	HC	5	10	4	4
	HC_{sub}	5	5		
76-80	HC	11	9	3	4
	HC_{sub}	9	9		
81-85	HC	8	9	1	-
	HC_{sub}	8	8		
86-90	HC	6	2	1	2
	HC_{sub}	2	2		
90-96	HC	1	1	1	2
	HC_{sub}	1	1		
Total	**HC**	**43**	**64**	**13**	**15**
	HC_{sub}	**37**	**37**		

DTI scans were processed in the subject space using FSL (FMRIB Software Library, University of Oxford) which is a comprehensive library of tools for brain imaging data analysis (Smith et al., 2004). Eddy-current-induced artefacts in the scans were corrected using the

'*eddy_correct*' command (Jenkinson et al., 2002). The skull was removed, and the brain extracted from the artefact-corrected image using the '*bet*' tool of FSL and visually verifying the output. Weighted fitting of the diffusion tensor on the brain was achieved using the '*dtifit*' command (Jenkinson et al., 2012) and four scalar maps – fractional anisotropy (FA), mean diffusivity (MD), radial diffusivity (RD) and axial diffusivity (AxD) – were computed from the Eigen values of the tensor.

2.1 Selection of corpus callosum segmentation strategy

The ADNI DTI data were acquired in the axial plane, so ROI delineation to segment the corpus callosum would ideally be performed in the same plane to obtain the most accurate measurements. However, the corpus callosum is not easily visualized in the axial plane, and in previous studies it has been segmented in the sagittal plane (Ardekani et al., 2014, Ota et al., 2006, Westerhausen et al., 2004). To address this constraint, we tested several strategies to segment the corpus callosum, comparing the results for atlas-based and manual segmentation in the sagittal plane with the data obtained from the axial acquisition plane (considered ground truth). A small group of ten subjects was sampled from the cohort for this purpose, to enable comparisons between strategies at an individual level. The result from this process was used to select the strategy for use with the full cohort.

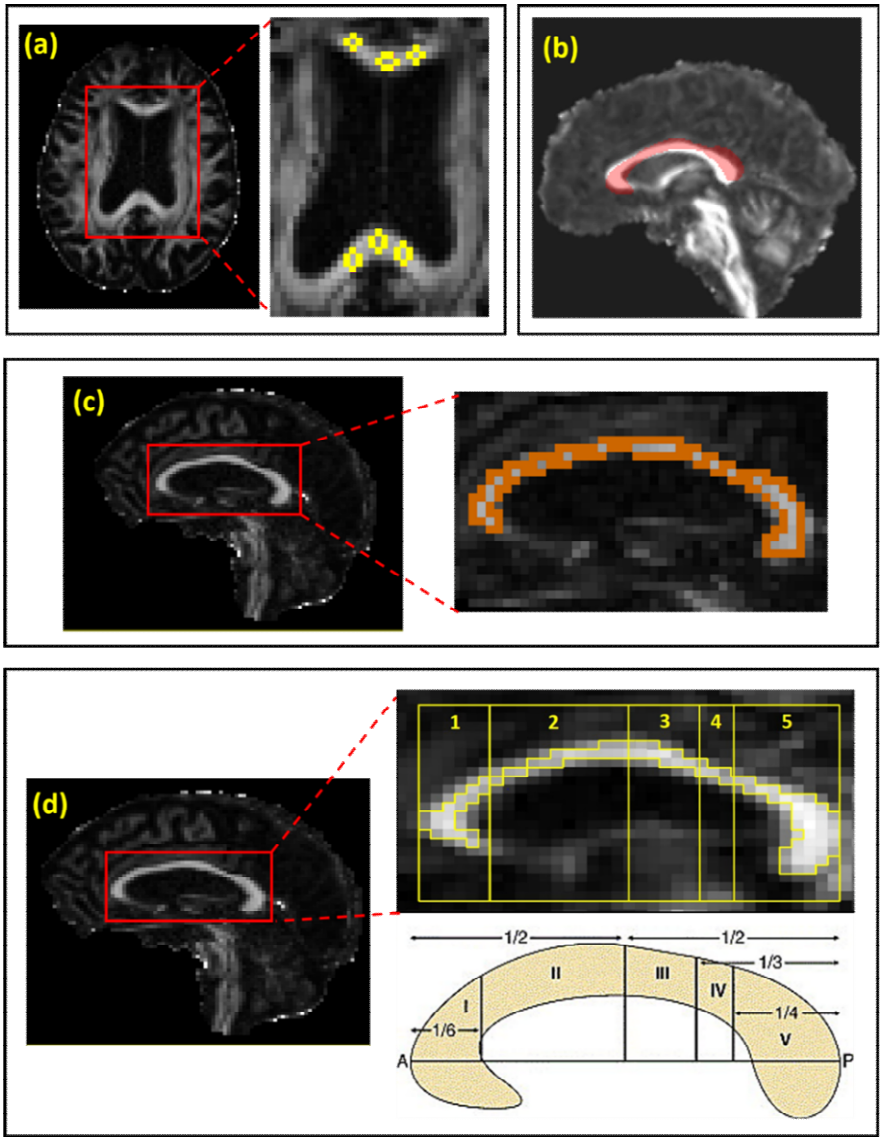

Figure 1: (a) Segmentation in the axial acquisition plane: circular ROIs (see inset) placed in the corpus callosum in the axial plane to sample median FA values to be used as ground truth; (b) Strategy using atlas-based mask of corpus callosum (ICBM-DTI-81 atlas) to estimate mean and median of pixel-wise values; (c) Strategy using manual segmentation of the corpus callosum on FA image reconstructed in the sagittal plane to estimate mean and median of pixel-wise values; (d) Extended manual segmentation of the corpus callosum in the sagittal plane into five pre-determined regions based on the Hofer and Frahm scheme (schematic adapted with permission from Hofer and Frahm (2006)).

Step 1: Measurement in the axial (acquisition) plane using circular ROIs on axial FA image: The corpus callosum was identified on axial FA maps using anatomical landmarks such as the ventricles. Segmenting the whole structure in the axial plane was not attempted, because poor boundary definition had strong potential to increase experimental uncertainty in the results. Instead, using the method illustrated in prior studies (Bartzokis et al. 2010, Li et al., 2009), FA values were sampled with circular ROIs of varying radii (to avoid partial volume effects), placed throughout all axial slices where the corpus callosum was clearly identifiable (Figure 1a, inset). Although previous studies have used the mean value from these ROIs, the heterogeneous distribution does not necessarily follow a normal distribution. Although mean and median values were very similar, checks on the individual distributions for the 10 subjects sampled for this step supported our use of the median to accommodate non-normal distributions of pixel FA values.

Step 2: Measurement using atlas-based delineation of ROI: The ICBM-DTI-81 atlas (Mori et al., 2008) provided with FSL, was used to obtain a mask of the corpus callosum using the labelled regions corresponding to the genu, the body and the splenium. Each subject's FA map was registered to the Montreal Neurological Institute (MNI) coordinate system (Figure 1b), and the mean and median values of FA were measured in the ROI using the mask.

Step 3: Measurement using manual delineation in the sagittal plane: In the manual segmentation approach, the FA image was first reconstructed in the sagittal plane, and the mid-sagittal slice of the brain was estimated using the method developed by

Freitas et al., 2011. Two slices each on either side of the mid-sagittal slice were segmented along with it to yield a volume of the corpus callosum consisting of five mid-sagittal slices (Figure 1c). The mean and the median of the FA values of the pixels in this ROI were estimated.

Fractional anisotropy (FA) values measured using the strategies of manual segmentation in the sagittal plane, and atlas-based segmentation, were compared to determine which gave values in best agreement with those obtained manually from the axial plane (which, as the plane of data acquisition, was treated as ground truth for the purpose of these comparisons).

For subsequent region-wise analysis, the corpus callosum was segmented into sub-regions in ImageJ, using the pre-defined fractions for the sagittal plane indicated in the Hofer and Frahm scheme (Hofer and Frahm, 2006) (Figure 1d). It is noted that while the corpus callosum is a bundle of fibres connecting the left and right hemispheres of the brain (Figure 1a), analysis using segmentation performed in the sagittal plane parsed this bundle of fibres cross-sectionally from anterior to posterior (Figure 1c), sampling its properties within a window of five sagittal slices.

Manual segmentation was performed in ROIEditor (Region of Interest Editing Tools v. 1.8). Statistical tests, including linear regression and ANCOVA for the variation in FA, MD, RD, and AxD with age, were conducted using software package R using other relevant factors such as gender and disease group as covariates. For region-wise analysis, measurements from each sub-region were tested separately. Measured parameter values and codes written in R to carry out the analyses are available at http://wrap.warwick.ac.uk/138931

3. Results and Discussion

3.1 Effects of gender on age-related changes not found significant in the cohort studied

To test for the effects of gender, multiple linear regression analyses of FA, MD, RD and AxD were carried out on cohort HC_{sub}. Age, gender, and the effect of their interaction were considered as factors. All four parameters exhibited linear trends with age in the age range analysed, in agreement with previously reported observations in the literature (Lebel et al., 2010; Ota et al., 2006). A consistent difference was observed between male and female patterns of changes with age, in regression plots of MD, RD and AxD, although this was not statistically significant. Such an offset was not observed for FA. The corresponding figures and regression equations are given in Figure S2 and Table S1 in Supplementary Materials. Since analysis of the HC_{sub} cohort did not indicate that gender was a statistically significant factor for DTI parameters as a function of age, subsequent analyses were conducted on the larger cohort HC using methods appropriate for application to differently sized study groups.

3.2 Comparison of corpus callosum segmentation methods

The results from the comparison of strategies for segmentation of the corpus callosum are shown in Figure 2. The primary constraint of the atlas-based ROI approach is evident in Figure 1b, where the mask of the corpus callosum is misaligned with the target structure evident in the image contrast. The mean and median of the FA in this ROI (Figure 2: Atlas ROI (mean) and Atlas ROI (median)) were estimated and compared with the manually-segmented axial data (ground truth) and manually-segmented regions in the reconstructed sagittal plane. Atlas-based measurements resulted in a significant reduction in the estimated mean and median FA, likely due to partial volume effects. Potential issues with accuracy in the ICBM-DTI-81 atlas are addressed in a prior study (Rohlfing 2013).

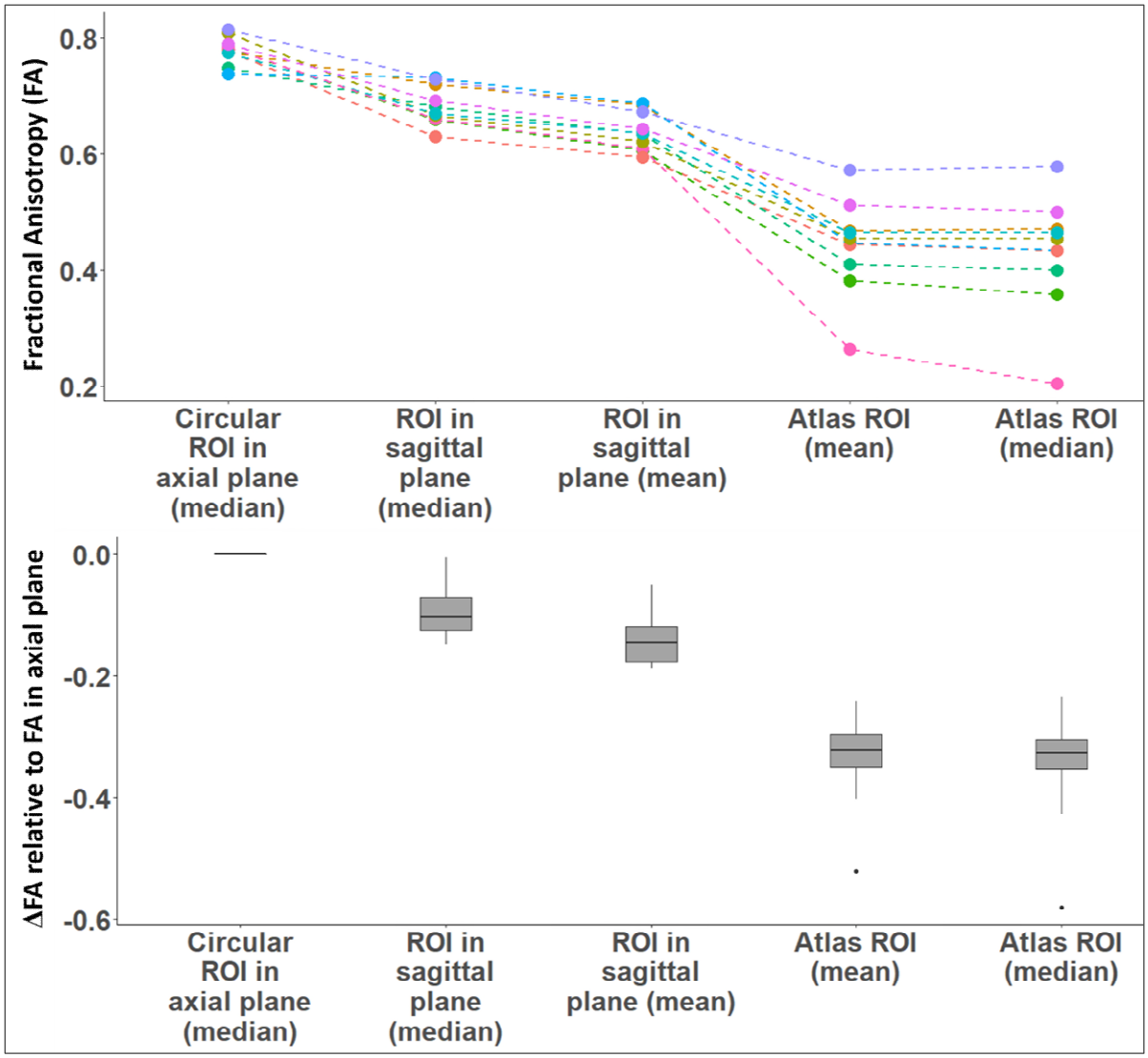

Figure 2: Measured values of FA in 10 subjects, using different segmentation schemes. Median of pixel-wise FA from multiple circular ROIs placed in the axial corpus callosum (Figure 1a) are considered ground truth. Corresponding box plots for each strategy show the distribution of offsets from ground truth for the 10 subjects. The experimental uncertainty in the data that can arise in subject comparisons from differences in scan sequence parameters (Zhu et al., 2009) has been avoided by only using images acquired using fully matched parameters; experimental uncertainty from other sources such as eddy current artefacts have been reduced by post-processing. In regions with high FA such as the corpus callosum, the reported experimental uncertainty in FA has been very small (Zhu et al., 2009).

By contrast, as shown in Figure 2, median values from the manually segmented ROI in the sagittal plane were closest to ground truth for the 10 sampled subjects. The slight offset of the FA values obtained manually in the sagittal plane compared to those from the axial plane may have arisen from i) the constrained sampling in the axial plane (reinforcing the need for ROI delineation in the sagittal plane), and/or from ii) interpolation errors arising from the sagittal reconstruction process. However, the similarity of the values, and the consistency of their distribution, indicated that this slight offset in the measured FA value would not affect the cohort-level relationships observed in subsequent regression analysis, and manual segmentation in the sagittal plane was subsequently used to obtain MD, RD, and AxD for the full cohort study.

3.3 Linear regression analysis of HC reveals age-related changes that vary between sub-regions, with evidence that axon diameters are a factor

Plots of linear regression analysis of FA, MD, RD and AxD on cohort HC, are shown in Figure 3. For all four diffusion parameters, age was a significant factor contributing to the changes observed ($p < 0.001$). Similar analyses were performed to investigate whether patterns of change with age were different in the sub-regions of corpus callosum (Figure 3e-h). (See Supplementary Materials for the corresponding regression equations.) Analysis of covariance (ANCOVA) revealed that the measured values of FA, MD, and RD differed significantly ($p < 0.001$) between the sub-regions when controlling for age (Table 2). Tukey's tests were performed for pairwise comparisons between the sub-regions for significantly differing values of the measured parameters (Figures 3 i-l). Estimates of the effect size of region on the distribution of FA, MD, RD, and AxD are shown in Table 2. Partial omega-squared (ω^2), being a bias-corrected effect size estimator, has been used to describe the effect sizes in this study.

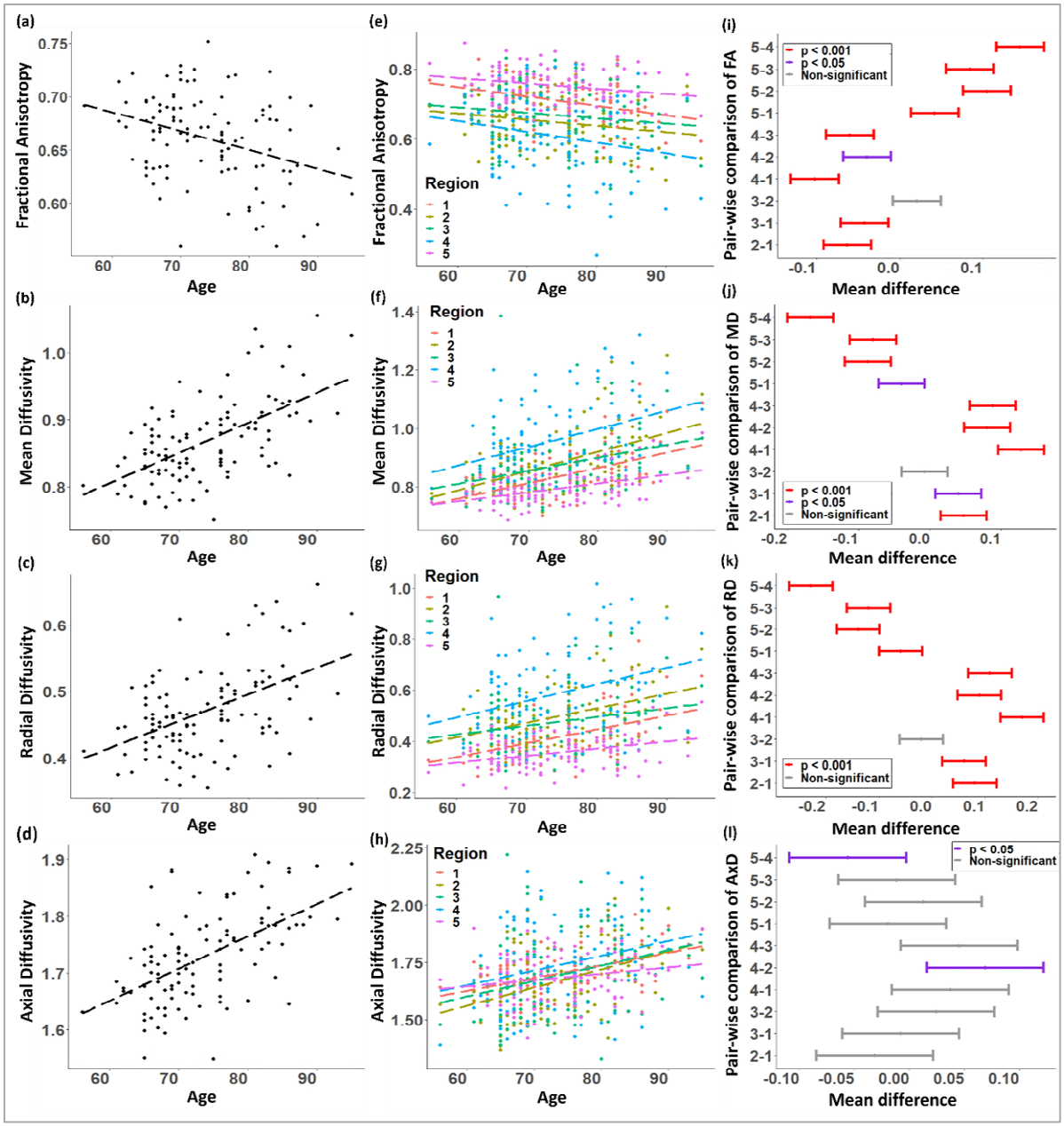

Figure 3: Scatter plots of DTI parameters versus age with linear regression lines: (a) fractional anisotropy, (b) mean diffusivity, (c) radial diffusivity, and (d) axial diffusivity in the whole corpus callosum. Figures (e)-(h) are the same type of scatter plots but stratified by corpus callosum sub-region. The significance of age as a contributing factor to the observed trends, and the r-squared values, have been given in the Supplementary Tables S2 and S3. Figures (i)-(l) show the results of Tukey's multiple comparison tests between regions, with colours indicating corresponding significance levels. Values of MD, RD, and AxD are in 10^{-3} mm^2/s.

When the effect or the sample size is small, ω^2 may carry negative values resulting from the bias correction (Okada, 2016).

A post-mortem study (Aboitiz et al., 1992) has shown that when parsing the corpus callosum cross-sectionally, the anterior region has the highest density of thin fibres. This starts decreasing towards the posterior regions and reaches a minimum before increasing again towards the posterior end. An opposite trend is observed for the density of fibres with a larger diameter. This density distribution of axonal diameter has been visualised in Figure 4a, in an ROI that provides a cross-sectional view of the corpus callosum. Another study (Barazany et al., 2009) has reported a positive correlation between RD and axon diameter in the corpus callosum of rat brain, potentially due to larger diameters leading to lower packing density and a subsequent increase in perpendicular diffusion. This relationship has been found to hold true in our study in the human corpus callosum as visualised in Figure 4b, even though we followed a different scheme of sub-division. The regional variations observed in DTI parameters in the cross-sectional corpus callosum ROI (Table 2) could likely be due to the varying density of axons with larger and smaller diameters that connect different regions of the two brain hemispheres (Figure 4a). An interesting finding here was that regional variations did not affect AxD values of the corpus callosum; this may be due to the relatively simpler and unidirectional nature of axons in the regions analysed. Our analysis suggests that variations in DTI properties between sub-regions in the corpus callosum are significant. Therefore, studies investigating the diffusion properties of corpus callosum in ageing or disease may be better served by analysing each sub-region separately. This has scope to reduce the variance observed in measured data, since our analysis indicates that at least 25% of variance can be explained by region-wise differences in the case of the parameters FA, MD, and RD (Table 2).

Table 2: Results of ANCOVA between regions 1 – 5 in HC, testing for the effects of regional differences after controlling for the effects of age.

Parameter	Cumulative p-value (ANCOVA)	ω^2
FA	< 0.001	0.295
MD	< 0.001	0.291
RD	< 0.001	0.330
AxD	0.006	0.019

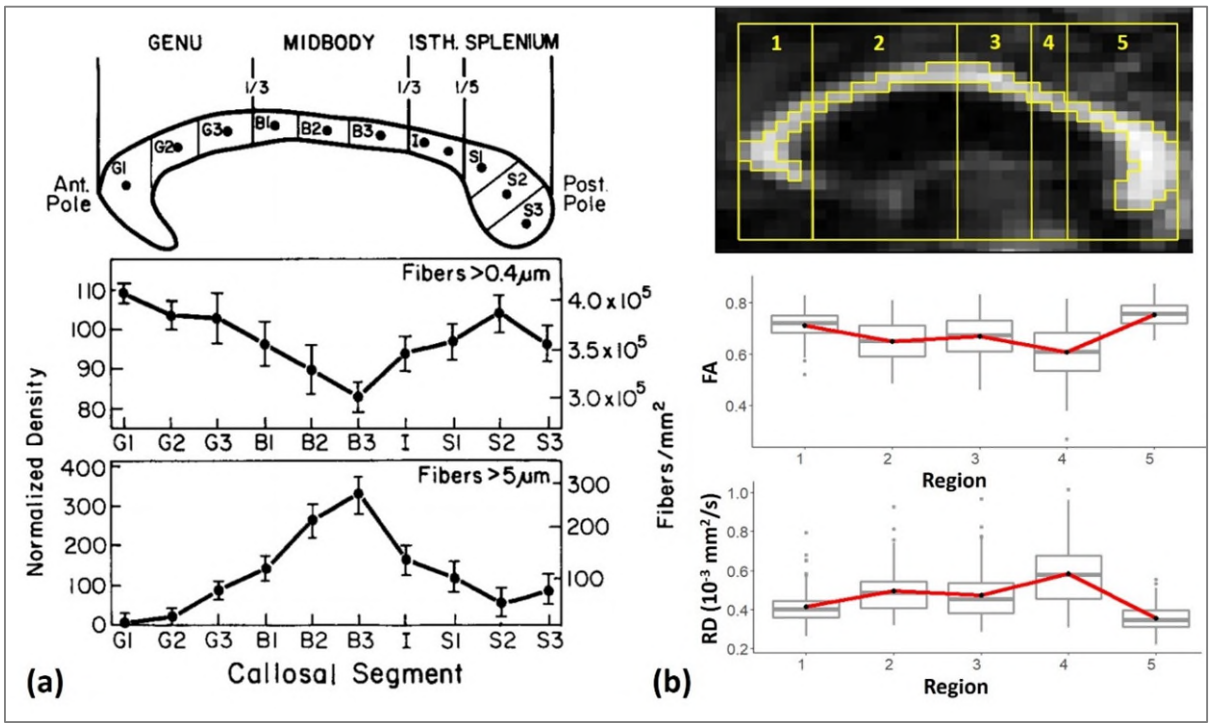

Figure 4: (a) Density distribution of small and large diameter axons in the corpus callosum; picture adapted with permission (Aboitiz et al., 1992). (b) Distribution of FA and RD values in the corpus callosum sub-regions were observed to follow a similar trajectory. Although the sub-division scheme used in this study is different to that used in (a), it can be observed that the minimum and maximum density for smaller and larger diameter fibres occur in region B3 (isthmus) which is approximately the same as region 4 in the Hofer scheme; where the minimum and maximum for FA and RD distributions have respectively been observed.

3.4 Comparison between MCI and healthy ageing: data indicating motor-related impairment in MCI reveal merits of corpus callosum analysis by sub-region

The effects of MCI on the corpus callosum and its sub-regions were investigated using data from cohorts HC and MCI (Figure 5). Initial tests were carried out on the whole corpus callosum ROI using ANCOVA (Figure 5a); they revealed subtle but significant differences between HC and MCI groups in FA, RD, and AxD, after controlling for the effects of age (Supplementary Table S4). Opposing changes in the magnitudes of RD and AxD (decrease and increase respectively), for patients with MCI compared to HC, may have masked any changes in MD (Supplementary Material Figure S3).

It is worth noting that the measured values for FA in MCI were higher than those for HC, and that the values for MD and RD were lower in MCI than for HC. This contradicts previous reports which showed trends of lower FA and higher diffusivities in degeneration (Amlien et al., 2013; Liu et al., 2013; Nowrangi et al., 2013; Wang et al., 2013), but seems to suggest a role for inflammation in MCI as indicated by increasing FA and decreasing diffusivities (Gupta et al., 2008; Nath et al., 2007; Renoux et al., 2006). This reportedly suggests either intracellular inflammation with inflow of extracellular water in the axons or decreased extracellular space due to cellular infiltration by inflammatory cells (Renoux et al., 2006). Neuroinflammation in MCI and Alzheimer's disease has not been extensively studied in this context. Advanced diffusion models of the brain such as those quantifying extracellular free-water volume are emerging markers being used to study neuro-inflammation (Pasternak et al., 2016, 2012), but are outside the scope of this study.

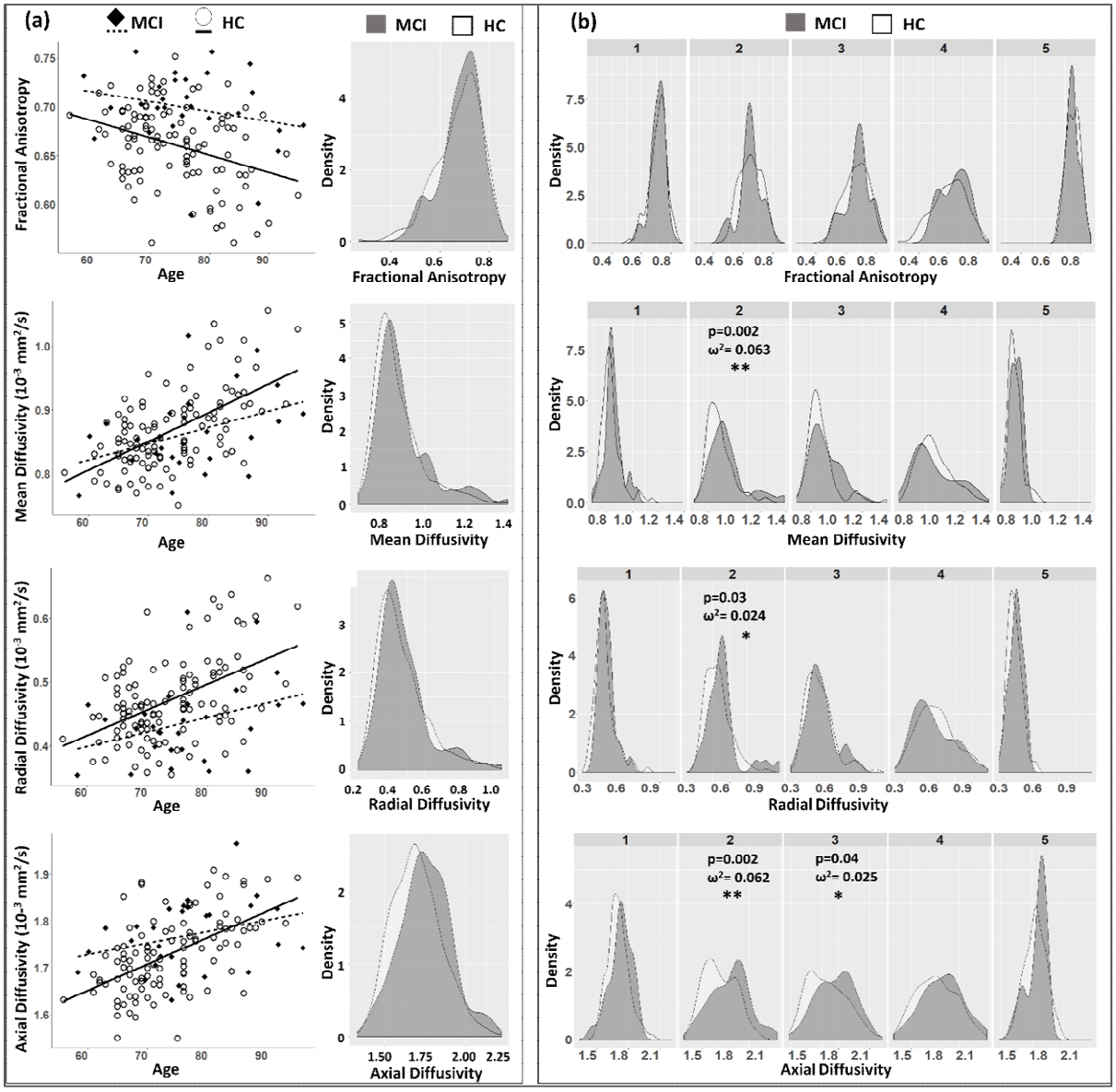

Figure 5: (a) Linear trends of FA, MD, RD and AxD, for HC and MCI groups, in the whole corpus callosum, with corresponding density plots (smoothed histograms) (b) Density plots of FA, MD, RD and AxD visualised separately in the corpus callosum sub-regions. Values of ω^2 and their p-values for differences in measurements between HC and MCI are shown on the plots where they were observed to be statistically significant. * denotes $p < 0.05$ and ** denotes $p < 0.01$. ω^2 and their p-values for the remaining figures have been given in Supplementary Tables S4 and S5. Values of MD, RD, and AxD are in 10^{-3} mm^2/s.

Investigation of region-specific measurements provided a better insight into differences between HC and MCI subjects (Figure 5b). Supplementary Table S5 summarises the results of analysis using ANCOVA, controlling for the effects of age. Values of MD, RD, and AxD differed significantly ($p < 0.05$) between HC and MCI in region 2, and that of AxD differed significantly ($p < 0.05$) in region 3. This indicates that degenerative changes observed in MCI are dominant in regions 2 and 3 of the corpus callosum; and that they may be more extensive in region 2 than in region 3. It must be noted that although the effect sizes of MCI in regions 2 and 3 for the significantly different DTI parameters (Supplementary Table S5) were higher than in other regions, their values were still small. This might be accounted for by subtle differences between HC and MCI during the early stages of cognitive impairment.

Physiological interpretations for RD have included demyelination, and that for AxD have included axonal degeneration (Song et al., 2002, 2003). They suggest that the corpus callosum integrity is likely to be diminished in MCI, potentially playing a role in progression to Alzheimer's disease. In a prior study with data from ADNI-2 participants, DTI properties in several white matter structures were compared for patients with MCI, Alzheimer's disease patients, and healthy controls (Nir et al., 2013). They found widespread anisotropy and diffusivity alterations in elderly patients with Alzheimer's disease. They also reported that diffusivity measures were more sensitive to microstructural alterations than FA and could detect subtle differences in patients with MCI compared to controls. This was supported by the results from the analysis of corpus callosum sub-regions in the present study that revealed alterations in MD, RD, and AxD between MCI and HC.

Region 2 of the corpus callosum projects to pre-motor and supplementary motor areas, and region 3 to primary motor areas of the brain (Hofer and Frahm, 2006). An effect of MCI, indicated by significantly different diffusivity measurements in regions 2 and 3 as reported in this study, may help explain motor impairments seen in MCI and pre-clinical Alzheimer's disease (Buchman and Bennett, 2011; de Paula et al., 2016; Förstl and Kurz, 1999; Wirths and Bayer, 2008). Neurophysiological examination data, accompanying individual ADNI-3 participant scans, was used to test this hypothesis. These data were collected as part of the screening process and provide preliminary information about a range of functional networks including motor, visual and auditory systems. They are summarised in Table 3 and show that a higher proportion of MCI subjects than HC were reported to show tremors, abnormal reflexes and impaired gait. It is interesting to note that this pattern was observed only in motor-related functions, and not in the results of visual or auditory examinations. This suggests that an impairment in motor skills is observed for MCI, supporting our results that indicate alterations in the corpus callosum regions projecting to motor areas of the brain.

The results of our study agree with data from previous studies (Snir et al., 2019; de Laat et al., 2011; Bhadelia et al., 2009) that show significant correlations between altered FA in the genu of the corpus callosum and abnormal gait function. It must be noted that our study found an increase in FA in these regions of interest whereas these studies report a decrease in FA. Due to the non-specific nature of DTI, it is difficult to establish the exact nature of pathological changes that may be occurring in the corpus callosum in MCI. A decrease in diffusivity values in regions 2 and 3 of the corpus callosum may indicate demyelination or axonal degeneration (Song et al., 2002, 2003), in the commissural tracts in the anterior parts of the corpus

callosum, resulting in diminished processing of information in the pre-motor, supplementary motor and primary motor areas of the brain.

Table 3: Summary of neurophysiological examinations of ADNI subjects, showing the percentage of subjects with abnormal results. The data shows an increase in motor-related abnormalities in MCI, compared to other functions tested.

Examination	**HC** % affected	**MCI** % affected
Visual impairment	5.6	3.6
Auditory impairment	6.5	7.1
Presence of tremors	8.4	21.4
Abnormal tendon reflexes	7.5	10.7
Abnormal plantar reflexes	0.9	3.6
Abnormal gait	8.4	21.4

4. Conclusions

Analysis of FA, MD, RD and AxD revealed that the properties of the corpus callosum are better characterised when segmented as five sub-regions, as opposed to as a single structure. Using this approach revealed changes in corpus callosum regions 2 and 3 of MCI subjects compared to HC, changes which were undetectable using the single ROI approach. The significance of the MCI-associated change is that regions 2 and 3 project to pre-motor, supplementary motor and motor areas of the brain. The DTI alterations in these regions were supported with evidence from ADNI-documented neurophysiological exams of these subjects, confirming that patients with MCI were more likely than HC to experience motor-related deficits,

compared to other impairments. A limitation to the interpretation of the neuroscience findings, enabled by the method adopted for this study, is the lack of detailed information about motor functions in the ADNI neurophysiological exams conducted as part of screening. The ADNI evaluations only indicate the presence or absence of abnormalities. Availability of detailed test results in the future may help estimate the correlation between DTI parameters, tremors, reflexes and gait, providing insight into the extent of the role of corpus callosum in motor impairment as observed in MCI and potentially, pre-clinical Alzheimer's disease.

In summary, we anticipate that the method demonstrated in this study will advance the detection in a clinical setting of alterations to the structure of the corpus callosum, and corresponding impacts on brain function, using this comparatively simple method to obtain the ROIs and supporting statistical analysis.

5. Acknowledgements

Data collection and sharing for this project was funded by the Alzheimer's Disease Neuroimaging Initiative (ADNI) (National Institutes of Health Grant U01 AG024904) and DOD ADNI (Department of Defense award number W81XWH-12-2-0012). ADNI is funded by the National Institute on Aging, the National Institute of Biomedical Imaging and Bioengineering, and through generous contributions from the following: AbbVie, Alzheimer's Association; Alzheimer's Drug Discovery Foundation; Araclon Biotech; BioClinica, Inc.; Biogen; Bristol-Myers Squibb Company; CereSpir, Inc.; Cogstate; Eisai Inc.; Elan Pharmaceuticals, Inc.; Eli Lilly and Company; EuroImmun; F. Hoffmann-La Roche Ltd and its affiliated company Genentech, Inc.; Fujirebio; GE Healthcare; IXICO Ltd.; Janssen Alzheimer Immunotherapy Research & Development, LLC.; Johnson & Johnson Pharmaceutical Research & Development LLC.;

Lumosity; Lundbeck; Merck & Co., Inc.; Meso Scale Diagnostics, LLC.; NeuroRx Research; Neurotrack Technologies; Novartis Pharmaceuticals Corporation; Pfizer Inc.; Piramal Imaging; Servier; Takeda Pharmaceutical Company; and Transition Therapeutics. The Canadian Institutes of Health Research is providing funds to support ADNI clinical sites in Canada. Private sector contributions are facilitated by the Foundation for the National Institutes of Health (www.fnih.org). The grantee organization is the Northern California Institute for Research and Education, and the study is coordinated by the Alzheimer's Therapeutic Research Institute at the University of Southern California. ADNI data are disseminated by the Laboratory for Neuro Imaging at the University of Southern California.

Computing facilities were provided by the Scientific Computing Research Technology Platform of the University of Warwick. The authors thank the University of Warwick, including the School of Engineering, for funding this research (SR). We also thank Jierong Luo, School of Engineering, University of Warwick, and Prof Keith D. White, Brain Rehabilitation Research Centre, University of Florida, for input to this study.

6. References

Aboitiz, F., Scheibel, A. B., Fisher, R. S., Zaidel, E., 1992. Fiber composition of the human corpus callosum. Brain Research 598, pp. 143–153.

Amlien, I. K., Fjell, A. M., Walhovd, K. B., Selnes, P., Stenset, V., Grambaite, R., Bjornerud, A., Due-Tonnessen, P., Skinningsrud, A., Gjerstad, L., Reinvang, I., Fladby, T., 2013. Mild cognitive impairment: cerebrospinal fluid tau biomarker pathologic levels and longitudinal changes in white matter integrity. Radiology 266, pp. 295–303.

Ardekani, B. A., Bachman, A. H., Figarsky, K., Sidtis, J. J., 2014. Corpus callosum shape changes in early Alzheimer's disease: an MRI study using the OASIS brain database. Brain Structure and Function 219, pp. 343–52.

Barazany, D., Basser, P. J., Assaf, Y., 2009. In vivo measurement of axon diameter distribution in the corpus callosum of rat brain. Brain 132, pp. 1210–20.

Bartzokis, G., Lu, P. H., Tingus, K., Mendez, M. F., Richard, A., Peters, D. G., Oluwadara, B., Barrall, K. A., Finn, J. P., Villablanca, P., Thompson, P. M., Mintz, J., 2010. Lifespan trajectory of myelin integrity and maximum motor speed. Neurobiology of Aging 31, pp. 1554–62.

Bennett, I. J., Greenia, D. E., Maillard, P., Sajjadi, S. A., DeCarli, C., Corrada, M. M., Kawas, C. H., 2017. Age-related white matter integrity differences in oldest-old without dementia. Neurobiology of Aging 56, pp. 108–114.

Bhadelia, R. A., Price, L. L., Tedesco, K. L., Scott, T., Qiu, W. Q., Patz, S., Folstein, M., Rosenberg, I., Caplan, L. R., Bergethon, P., 2009. Diffusion tensor imaging, white matter lesions, the corpus callosum, and gait in the elderly. Stroke 40, pp. 3816–20.

Buchman, A. S., Bennett, D. A., 2011. Loss of motor function in preclinical Alzheimer's disease. Expert Review of Neurotherapeutics 11, pp. 665–676.

Clarke, J. M., Zaidel, E., 1994. Anatomical-behavioral relationships: corpus callosum morphometry and hemispheric specialization. Behavioural Brain Research 64, pp. 185–202.

de Laat, K. F., Tuladhar, A. M., van Norden, A. G., Norris, D. G., Zwiers, M. P., de Leeuw, F. E., 2011. Loss of white matter integrity is associated with gait disorders in cerebral small vessel disease. Brain 134, pp. 73–83.

de Paula, J. J., Albuquerque, M. R., Lage, G. M., Bicalho, M. A., Romano-Silva, M. A., Malloy-Diniz, L. F., 2016. Impairment of fine motor dexterity in mild cognitive impairment and

Alzheimer’s disease dementia: association with activities of daily living. Brazilian Journal of Psychiatry 38, pp. 235–8.

de Schotten, M. T., Bizzi, A., Dell'Acqua, F., Allin, M., Walshe, M., Murray, R., Williams, S. C., Murphy, D. G. and Catani, M., 2011. Atlasing location, asymmetry and inter-subject variability of white matter tracts in the human brain with MR diffusion tractography. Neuroimage, 54(1), pp.49-59.

Decker, B. M., Guitar, B., Solomon, A., 2018. Corpus callosum demyelination associated with acquired stuttering. BMJ Case Reports 2018.

Denenberg, V. H., Kertesz, A., Cowell, P. E., 1991. A factor analysis of the human’s corpus callosum. Brain Research 548, pp. 126–32.

Evangelou, N., Konz, D., Esiri, M. M., Smith, S., Palace, J., Matthews, P.M., 2000. Regional axonal loss in the corpus callosum correlates with cerebral white matter lesion volume and distribution in multiple sclerosis. Brain 123 (9), pp. 1845–9.

Feng, Q., Liao, Z., Jiang, H., Mao, D., Wang, M., Yu, E., Ding, Z., 2018. Corpus callosum radiomics-based classification model in Alzheimer’s disease: a case-control study. Frontiers in Neurology 9, 618.

Förstl, H., Kurz, A., 1999. Clinical features of Alzheimer's disease. European Archives of Psychiatry and Clinical Neuroscience 249, pp. 288–290.

Freitas, P., Rittner, L., Appenzeller, S., Lotufo, R., 2011. Watershed-based segmentation of the midsagittal section of the corpus callosum in diffusion MRI, in: 2011 24th SIBGRAPI Conference on Graphics, Patterns and Images, IEEE. pp. 274–280.

Goldman, J G, Bledsoe, I O, Merkitch, D, Dinh, V, Bernard, B, Stebbins, G T, 2017. Corpus callosal atrophy and associations with cognitive impairment in Parkinson disease. Neurology 88 (13), 1265–1272.

Granberg, T, Martola, J, Bergendal, G, Shams, S, Damangir, S, Aspelin, P, Fredrikson, S, Kristoffersen-Wiberg, M, 2015. Corpus callosum atrophy is strongly associated with cognitive impairment in multiple sclerosis: Results of a 17-year longitudinal study. Multiple Sclerosis Journal 21, 1151–8.

Gupta, R. K., Nath, K., Prasad, A., Prasad, K. N., Husain, M., Rathore, R. K., Husain, N., Srivastava, C., Khetan, P., Trivedi, R., Narayana, P. A., 2008. In vivo demonstration of neuroinflammatory molecule expression in brain abscess with diffusion tensor imaging. American Journal of Neuroradiology 29, pp. 326–32.

Hasan, K. M., Gupta, R. K., Santos, R. M., Wolinsky, J. S., Narayana, P. A., 2005. Diffusion tensor fractional anisotropy of the normal-appearing seven segments of the corpus callosum in healthy adults and relapsing-remitting multiple sclerosis patients. Journal of Magnetic Resonance Imaging 21, pp. 735–43.

Hofer, S., Frahm, J., 2006. Topography of the human corpus callosum revisited–comprehensive fiber tractography using diffusion tensor magnetic resonance imaging. NeuroImage 32, pp. 989–94.

Hou, J., Pakkenberg, B., 2012. Age-related degeneration of corpus callosum in the 90+ years measured with stereology. Neurobiology of Aging 33, 1009-e1.

Jenkinson, M., Bannister, P., Brady, M., Smith, S., 2002. Improved optimization for the robust and accurate linear registration and motion correction of brain images. NeuroImage 17, pp. 825–841.

Jenkinson, M., Beckmann, C. F., Behrens, T. E., Woolrich, M. W., Smith, S. M., 2012. FSL. NeuroImage 62, pp. 782–90.

Kanaan, R. A., Allin, M., Picchioni, M., Barker, G. J., Daly, E., Shergill, S. S., Woolley, J., McGuire, P. K., 2012. Gender differences in white matter microstructure. PloS one, 7(6).

Køster, R N, Jesper, R, Bente, P, 2018. The total number of myelinated nerve fibers is reduced in corpus callosum in brains from patients with Alzheimer's disease. Neurobiol. Aging 69, 58–64.

Landman, B. A., Farrell, J. A., Jones, C. K., Smith, S. A., Prince, J. L., Mori, S., 2007. Effects of diffusion weighting schemes on the reproducibility of DTI-derived fractional anisotropy, mean diffusivity, and principal eigenvector measurements at 1.5 T. NeuroImage 36, pp. 1123–38.

Laws, K. R., Irvine, K., Gale, T. M., 2018. Sex differences in Alzheimer's disease. Current opinion in psychiatry, 31(2), pp.133-139.

Le Bihan, D., Mangin, J. F., Poupon, C., Clark, C. A., Pappata, S., Molko, N., Chabriat, H., 2001. Diffusion tensor imaging: Concepts and applications. Journal of Magnetic Resonance Imaging 13, pp. 534–546.

Lebel, C., Caverhill-Godkewitsch, S., Beaulieu, C., 2010. Age-related regional variations of the corpus callosum identified by diffusion tensor tractography. NeuroImage 52, pp. 20–31.

Lee, S. H., Bachman, A. H., Yu, D., Lim, J., Ardekani, B. A., 2016. Predicting progression from mild cognitive impairment to Alzheimer's disease using longitudinal callosal atrophy. Alzheimer's & Dementia 2, pp. 68–74.

Li, T. Q., Yao, B., van Gelderen, P., Merkle, H., Dodd, S., Talagala, L., Koretsky, A. P., Duyn, J., 2009. Characterization of T2* heterogeneity in human brain white matter. Magnetic Resonance in Medicine 62, pp. 1652–1657.

Lin, K. A., Choudhury, K. R., Rathakrishnan, B. G., Marks, D. M., Petrella, J. R., Doraiswamy, P. M., Alzheimer's Disease Neuroimaging Initiative, 2015. Marked gender

differences in progression of mild cognitive impairment over 8 years. Alzheimer's & dementia: translational research & clinical interventions, 1(2), pp.103-110.

Liu, J., Yin, C., Xia, S., Jia, L., Guo, Y., Zhao, Z., Li, X., Han, Y., Jia, J., 2013. White matter changes in patients with amnestic mild cognitive impairment detected by diffusion tensor imaging. PLoS One 8 (3), e59440.

Ma, L., Hasan, K. M., Steinberg, J. L., Narayana, P. A., Lane, S. D., Zuniga, E. A., Kramer, L. A., Moeller, F. G., 2009. Diffusion tensor imaging in cocaine dependence: regional effects of cocaine on corpus callosum and effect of cocaine administration route. Drug and Alcohol Dependence 104, pp. 262–267.

Mann, D. M., Oliver, R., Snowden, J. S., 1993. The topographic distribution of brain atrophy in Huntington's disease and progressive supranuclear palsy. Acta Neuropathologica 85, pp. 553–9.

Marner, L., Nyengaard, J. R., Tang, Y., Pakkenberg, B., 2003. Marked loss of myelinated nerve fibers in the human brain with age. The Journal of Comparative Neurology 462, pp. 144–52.

Mori, S., Oishi, K., Jiang, H., Jiang, L., Li, X., Akhter, K., Hua, K., Faria, A. V., Mahmood, A., Woods, R., et al., 2008. Stereotaxic white matter atlas based on diffusion tensor imaging in an ICBM template. NeuroImage 40, pp. 570–582.

Nath, K., Husain, M., Trivedi, R., Kumar, R., Prasad, K. N., Rathore, R. K., Gupta, R. K., 2007. Clinical implications of increased fractional anisotropy in meningitis associated with brain abscess. Journal of Computer Assisted Tomography 31, pp. 888–93.

Nir, T. M., Jahanshad, N., Villalon-Reina, J. E., Toga, A. W., Jack Jr., C. R., Weiner, M. W., Thompson, P. M., Alzheimer's Disease Neuroimaging Initiative, 2013. Effectiveness of

regional DTI measures in distinguishing Alzheimer's disease, MCI, and normal aging. NeuroImage: Clinical 3, pp. 180–195.

Nowrangi, M. A., Lyketsos, C. G., Leoutsakos, J. M., Oishi, K., Albert, M., Mori, S., Mielke, M. M., 2013. Longitudinal, region-specific course of diffusion tensor imaging measures in mild cognitive impairment and Alzheimer's disease. Alzheimer's & Dementia 9, pp. 519–28.

Okada, K., 2016. Negative estimate of variance-accounted-for effect size: How often it is obtained, and what happens if it is treated as zero. Behavior Research Methods 49, pp. 979-87.

Ota, M., Obata, T., Akine, Y., Ito, H., Ikehira, H., Asada, T., Suhara, T., 2006. Age-related degeneration of corpus callosum measured with diffusion tensor imaging. NeuroImage 31, pp. 1445–52.

Pardoe, H. R., Mandelstam, S. A., Hiess, R. K., Kuzniecky, R. I., Jackson, G. D., Alzheimer's Disease Neuroimaging Initiative, Epilepsy Phenome/Genome Project Investigators, 2015. Quantitative assessment of corpus callosum morphology in periventricular nodular heterotopia. Epilepsy Research 109, pp. 40–7.

Pasternak, O., Kubicki, M., Shenton, M. E., 2016. In vivo imaging of neuroinflammation in schizophrenia. Schizophrenia Research 173, pp. 200–212.

Pasternak, O., Westin, C. F., Bouix, S., Seidman, L. J., Goldstein, J. M., Woo, T. U., Petryshen, T. L., Mesholam-Gately, R. I., McCarley, R. W., Kikinis, R., Shenton, M. E., Kubicki, M., 2012. Excessive extracellular volume reveals a neurodegenerative pattern in schizophrenia onset. The Journal of Neuroscience 32, pp. 17365–72.

Peters, M., Oeltze, S., Seminowicz, D., Steinmetz, H., Koeneke, S., Jancke, L., 2002. Division of the corpus callosum into subregions. Brain and Cognition 50, pp. 62–72.

Piguet, O., Double, K. L., Kril, J. J., Harasty, J., Macdonald, V., McRitchie, D. A., Halliday, G. M., 2009. White matter loss in healthy ageing: a postmortem analysis. Neurobiology of Aging 30, pp. 1288–95.

Prendergast, D. M., Ardekani, B., Ikuta, T., John, M., Peters, B., DeRosse, P., Wellington, R., Malhotra, A. K., Szeszko, P. R., 2015. Age and sex effects on corpus callosum morphology across the lifespan. Human Brain Mapping 36, pp. 2691–702.

Renoux, J., Facon, D., Fillard, P., Huynh, I., Lasjaunias, P., Ducreux, D., 2006. MR diffusion tensor imaging and fiber tracking in inflammatory diseases of the spinal cord. American Journal of Neuroradiology 27, pp. 1947–51.

Reuter-Lorenz, P. A., Stanczak, L., 2000. Differential effects of aging on the functions of the corpus callosum. Developmental Neuropsychology 18, pp. 113–37.

Rohlfing, T., 2013. Incorrect ICBM-DTI-81 atlas orientation and white matter labels. Frontiers in Neuroscience 7.

Sala, S., Agosta, F., Pagani, E., Copetti, M., Comi, G., Filippi, M., 2012. Microstructural changes and atrophy in brain white matter tracts with aging. Neurobiology of Aging 33, pp. 488–498.

Shahab, S, Stefanik, L, Foussias, G, Lai, M C, Anderson, K K, Voineskos, A N, 2018. Sex and diffusion tensor imaging of white matter in schizophrenia: A systematic review plus meta-analysis of the corpus callosum. Schizophrenia Bulletin 44, 203–221.

Smith, S. M., Jenkinson, M., Woolrich, M. W., Beckmann, C. F., Behrens, T. E., Johansen-Berg, H., Bannister, P. R., De Luca, M., Drobnjak, I., Flitney, D. E., Niazy, R. K., Saunders, J., Vickers, J., Zhang, Y., De Stefano, N., Brady, J. M., Matthews, P. M., 2004. Advances in functional and structural MR image analysis and implementation as FSL. NeuroImage 23 Suppl 1, pp. S208–19.

Snir, J. A., Bartha, R., Montero-Odasso, M., 2019. White matter integrity is associated with gait impairment and falls in mild cognitive impairment. Results from the gait and brain study. NeuroImage: Clinical 29.

Song, S. K., Sun, S. W., Ju, W. K., Lin, S. J., Cross, A. H., Neufeld, A. H., 2003. Diffusion tensor imaging detects and differentiates axon and myelin degeneration in mouse optic nerve after retinal ischemia. NeuroImage 20, pp. 1714–22.

Song, S. K., Sun, S. W., Ramsbottom, M. J., Chang, C., Russell, J., Cross, A. H., 2002. Dysmyelination revealed through MRI as increased radial (but unchanged axial) diffusion of water. NeuroImage 17, pp. 1429–1436.

Sullivan, E. V., Adalsteinsson, E., Hedehus, M., Ju, C., Moseley, M., Lim, K. O., Pfefferbaum, A., 2001. Equivalent disruption of regional white matter microstructure in ageing healthy men and women. Neuroreport 12, pp. 99–104.

Sullivan, E. V., Pfefferbaum, A., 2003. Diffusion tensor imaging in normal aging and neuropsychiatric disorders. European Journal of Radiology 45, pp. 244–255.

Sullivan, E. V., Rosenbloom, M. J., Desmond, J. E., Pfefferbaum, A., 2001b. Sex differences in corpus callosum size: relationship to age and intracranial size. Neurobiology of Aging 22, pp. 603–11.

van der Knaap, L. J., van der Ham, I. J., 2011. How does the corpus callosum mediate interhemispheric transfer? A review. Behavioural Brain Research 223, pp. 211–21.

Wang, J. H., Lv, P. Y., Wang, H. B., Li, Z. L., Li, N., Sun, Z. Y., Zhao, B. H., Huang, Y., 2013. Diffusion tensor imaging measures of normal appearing white matter in patients who are aging, or have amnestic mild cognitive impairment, or Alzheimer's disease. Journal of Clinical Neuroscience 20, pp. 1089–94.

Wang, X. D., Ren, M., Zhu, M. W., Gao, W. P., Zhang, J., Shen, H., Lin, Z. G., Feng, H. L., Zhao, C. J., Gao, K., 2015a. Corpus callosum atrophy associated with the degree of cognitive decline in patients with Alzheimer's dementia or mild cognitive impairment: a meta-analysis of the region of interest structural imaging studies. Journal of Psychiatric Research 63, pp. 10–9.

Wang, Z., Wang, J., Zhang, H., Mchugh, R., Sun, X., Li, K., Yang, Q. X., 2015b. Interhemispheric functional and structural disconnection in Alzheimer's disease: a combined resting-state FMRI and DTI study. PLoS One 10, e0126310.

Westerhausen, R., Kreuder, F., Sequeira, S. S., Walter, C., Woerner, W., Wittling, R. A., Schweiger, E. and Wittling, W., 2004. Effects of handedness and gender on macro-and microstructure of the corpus callosum and its subregions: a combined high-resolution and diffusion-tensor MRI study. Cognitive brain research, 21(3), pp. 418-426.

Wirths, O., Bayer, T. A., 2008. Motor impairment in Alzheimer's disease and transgenic Alzheimer's disease mouse models. Genes, Brain and Behavior 7 Suppl 1, pp. 1–5.

Witelson, S. F., 1989. Hand and sex differences in the isthmus and genu of the human corpus callosum: a postmortem morphological study. Brain 112 (3), pp. 799–835.

Wolff, J. J., Gerig, G., Lewis, J. D., Soda, T., Styner, M. A., Vachet, C., Botteron, K.N., Elison, J. T., Dager, S. R., Estes, A. M., Hazlett, H. C., Schultz, R. T., Zwaigenbaum, L., Piven, J., Network, I., 2015. Altered corpus callosum morphology associated with autism over the first 2 years of life. Brain 138, pp. 2046–58.

Woodruff, P. W., McManus, I. C., David, A. S., 1995. Meta-analysis of corpus callosum size in schizophrenia. Journal of Neurology, Neurosurgery, and Psychiatry 58, pp. 457–61.

Xiu, Y., Kong, X. R., Zhang, L., Qiu, X., Gao, Y., Huang, C. X., Chao, F. L., Wang, S. R., Tang, Y., 2015. The myelinated fiber loss in the corpus callosum of mouse model of schizophrenia induced by MK-801. Journal of Psychiatric Research 63, pp. 132–40.

Zavaliangos-Petropulu, A., Nir, T. M., Thomopoulos, S. I., Reid, R. I., Bernstein, M. A., Borowski, B., Jack Jr, C. R., Weiner, M. W., Jahanshad, N., Thompson, P. M., 2019. Diffusion MRI indices and their relation to cognitive impairment in brain aging: The updated multi-protocol approach in ADNI3. Frontiers in Neuroinformatics 13.

Zhu, T., Liu, X., Gaugh, M. D., Connelly, P. R., Ni, H., Ekholm, S., et al., 2009. Evaluation of measurement uncertainties in human diffusion tensor imaging (DTI)-derived parameters and optimization of clinical DTI protocols with a wild bootstrap analysis. Journal of Magnetic Resonance Imaging 29, pp. 422–435.

Supplementary Material

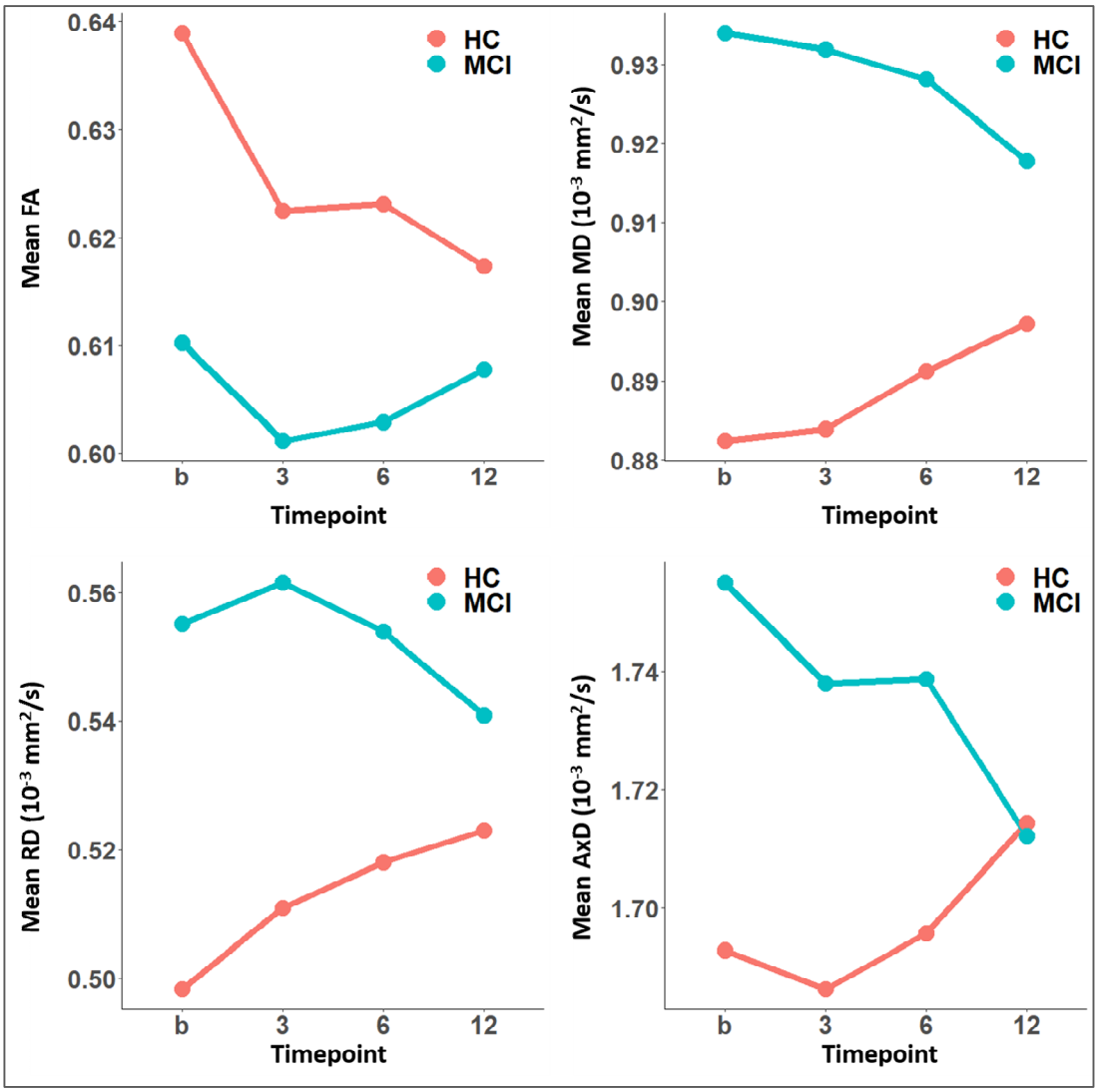

Figure S1: Results of a longitudinal analysis of DTI images of age-matched 14 HC and 14 MCI subjects between 65 and 75 years old from ADNI-2, acquired with the same set of scan parameters. The plots show the trajectories of average FA, MD, RD, and AxD values for each cohort over a time period of 1 year. 'b' denotes baseline, '3', '6', and '12' denote a 3-month, 6-month, and 12-month follow-up after the baseline visit. Although the longitudinal analysis gives a valuable insight into differences between HC and MCI cohorts, this is limited to a 1-year time span. Moreover, the results indicate a pattern of change with respect to the baseline, and not with the participant age itself.

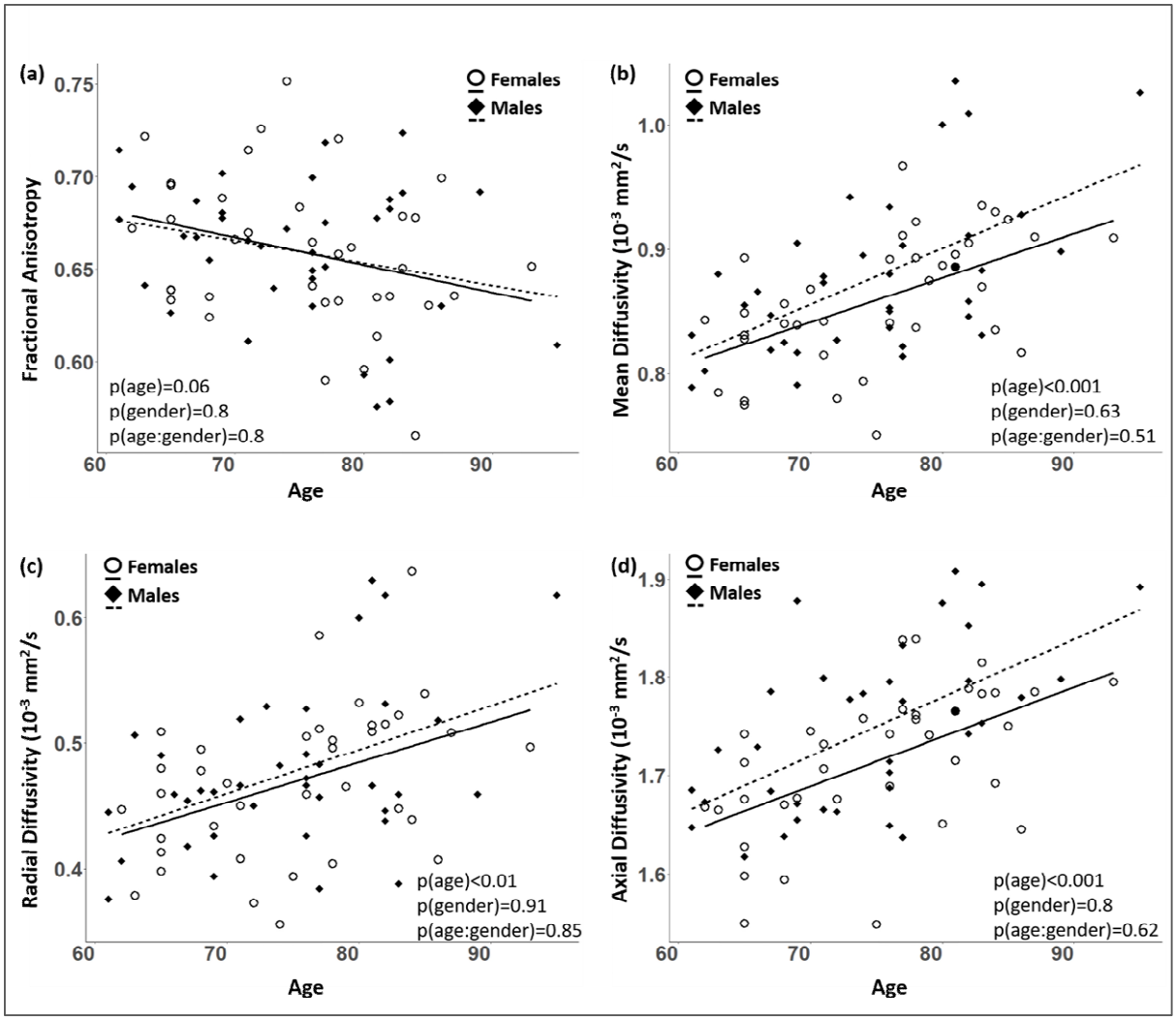

Figure S2: Multiple regression plots of (a) fractional anisotropy (FA), (b) mean diffusivity (MD), (c) radial diffusivity (RD), and (d) axial diffusivity (AxD) in the corpus callosum of subjects from cohort HC_{sub}. The contribution of each factor, i.e., age, gender and their interaction, to the observed linear relationship is tested using the null hypothesis about its correlation with the DTI parameters; an output p-value is obtained based on testing the null hypothesis that the factor has no effect. The factor is considered significant if 'p' is less than 0.05. p(age:gender) denotes the p-value for the effect of interaction of age and gender on the DTI parameters.

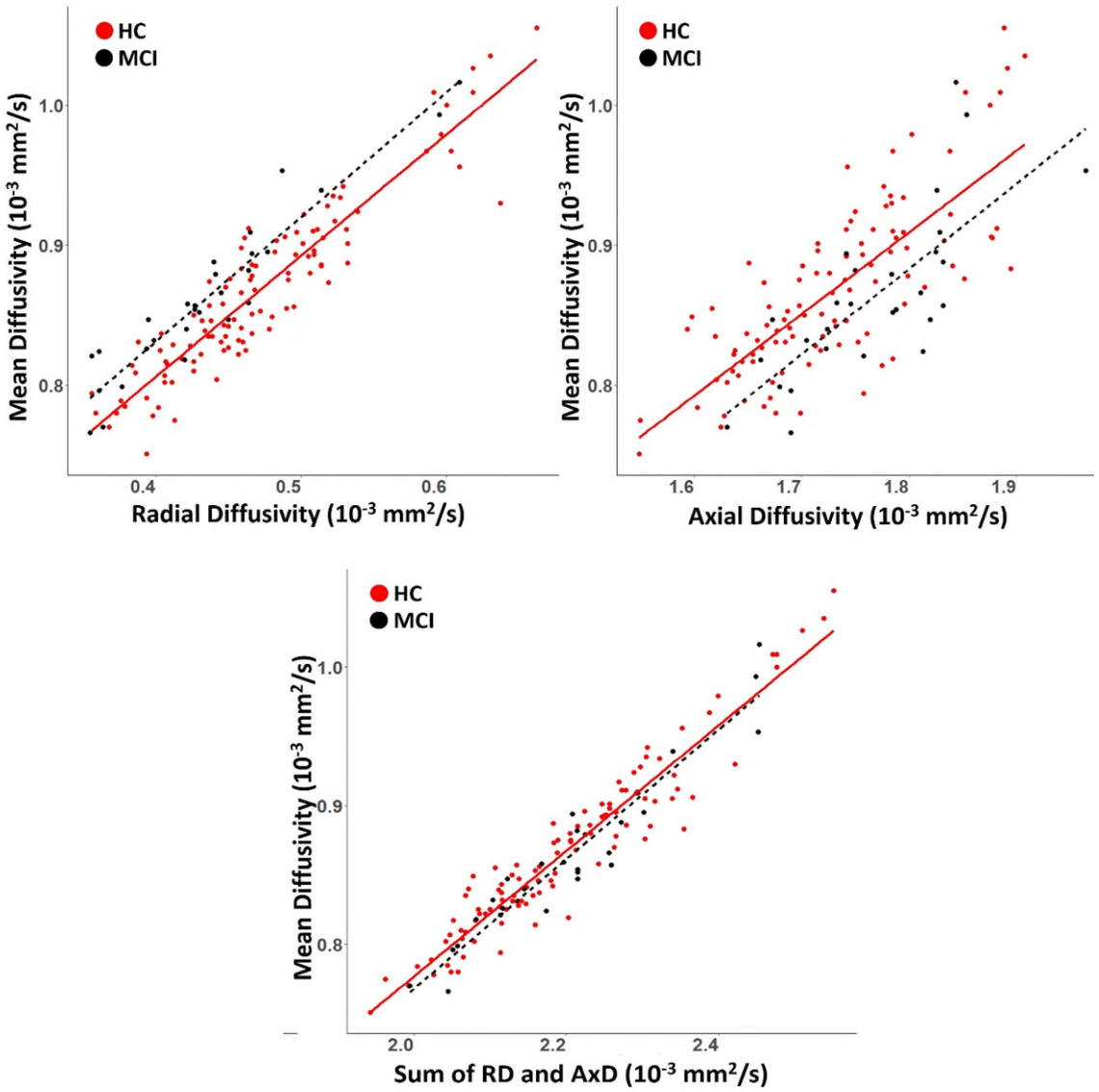

Figure S3: Plots showing the relationships between MD, RD and AxD of HC and MCI subjects. Equations using diffusion tensor eigen values, RD = $(\lambda_2 + \lambda_3)/2$, AxD = λ_1 and MD = $(\lambda_1 + \lambda_2 + \lambda_3)/3$, imply a linear relationship between MD and RD + AxD. These equations are used to generate plots that show a decrease in RD and an increase in AxD in MCI individuals compared to HC, for a given value of MD. The plot on the right suggests that these opposing patterns (represented by RD + AxD) bring the MD values of HC and MCI subjects closer to each other, resulting in a non-significant difference.

Table S1: Linear regression equations modelling ageing in the corpus callosum of subjects in HC_{sub}, stratified by gender.

DTI parameter	Males	Females
Fractional anisotropy	0.75 – 0.0012 * age	0.77 – 0.0015 * age
Mean diffusivity	0.54 + 0.0045 * age	0.59 + 0.0036 * age
Radial diffusivity	0.22 + 0.0035 * age	0.23 + 0.0032 * age
Axial diffusivity	1.3 + 0.006 * age	1.34 + 0.005 * age

Table S2: Linear regression equations modelling ageing in the whole corpus callosum ROI of subjects in cohort HC.

DTI parameter	Equation	r^2	p-value
Fractional anisotropy	0.79 – 0.0018 * age	0.11	< 0.001
Mean diffusivity	0.53 + 0.0045 * age	0.34	< 0.001
Radial diffusivity	0.18 + 0.004 * age	0.23	< 0.001
Axial diffusivity	1.31 + 0.0057 * age	0.3	< 0.001

Table S3: Linear regression equations modelling ageing in the corpus callosum sub-regions of subjects in cohort HC.

DTI parameter	**Region 1**	**r^2**	**p-value**
FA	0.9 – 0.0026* age	0.12	< 0.001
MD	0.44 + 0.0052 * age	0.29	< 0.001
RD	0.01 + 0.0054 * age	0.23	0.84
AxD	1.29 + 0.0055 * age	0.19	< 0.001
DTI parameter	**Region 2**	**r^2**	**p-value**
FA	0.78 – 0.0017 * age	0.028	< 0.001
MD	0.39 + 0.0065 * age	0.27	< 0.001
RD	0.07 + 0.0056 * age	0.16	0.42
AxD	1.08 + 0.0079 * age	0.17	< 0.001
DTI parameter	**Region 3**	**r^2**	**p-value**
FA	0.78 – 0.0015 * age	0.012	< 0.001
MD	0.54 + 0.0044 * age	0.102	< 0.001
RD	0.22 + 0.0034 * age	0.04	< 0.05
AxD	1.19 + 0.0067 * age	0.07	< 0.001
DTI parameter	**Region 4**	**r^2**	**p-value**
FA	0.84 – 0.003 * age	0.04	< 0.001
MD	0.49 + 0.0062 * age	0.15	< 0.001
RD	0.1 + 0.0065 * age	0.1	0.5
AxD	1.27 + 0.0064 * age	0.07	< 0.001
DTI parameter	**Region 5**	**r^2**	**p-value**
FA	0.86 – 0.0015 * age	0.05	< 0.001
MD	0.56 + 0.003 * age	0.19	< 0.001
RD	0.15 + 0.0027 * age	0.115	< 0.01
AxD	1.47 + 0.0027 * age	0.04	< 0.001

Table S4: Linear regression equations modelling ageing in the whole corpus callosum ROI of subjects in cohort MCI (corresponding equations for cohort HC given in Table S2). Here r^2 denotes the proportion of variance in the DTI parameters explained by age through linear regression modelling (data includes subjects from both HC and MCI cohorts). ω^2 denotes the effect size of disease (MCI) in the DTI parameter, with a significance level denoted by the corresponding p-value.

Parameter	**MCI equation**	**r^2**	**ω^2**	**p-value**
FA	0.77 – 0.001 * age	0.02	0.13	< 0.001
MD	0.67 + 0.0025 * age	0.13	-0.006	0.68
RD	0.26 + 0.0022 * age	0.08	0.05	< 0.01
AxD	1.57 + 0.0024 * age	0.06	0.042	< 0.01

Table S5: Linear regression equations modelling ageing in the whole corpus callosum ROI of subjects in cohort MCI. r^2 denotes the proportion of variance in the DTI parameter explained by age through linear regression modelling. ω^2 denotes the effect size of disease (MCI) in the DTI parameter, with a significance level denoted by the corresponding p-value.

Parameter	**Region 1 MCI equation**	**r^2**	**ω^2**	**p-value**
FA	0.82 – 0.0013 * age	0.035	-0.007	0.89
MD	0.62 + 0.003 * age	0.12	0.004	0.21
RD	0.21 + 0.002 * age	0.11	-0.001	0.35
AxD	1.55 + 0.002 * age	0.002	0.003	0.24
Parameter	**Region 2 MCI equation**	**r^2**	**ω^2**	**p-value**
FA	0.817 – 0.002 * age	0.04	-0.006	0.7
MD	0.55 + 0.005 * age	0.076	0.063	< 0.005
RD	0.109 + 0.005 * age	0.082	0.024	< 0.05
AxD	1.52 + 0.003 * age	0	0.062	< 0.005
Parameter	**Region 3 MCI equation**	**r^2**	**ω^2**	**p-value**
FA	0.8 – 0.0015 * age	0	-0.004	0.47
MD	0.77 + 0.002 * age	0	0.012	0.11
RD	0.33 + 0.002 * age	0	-0.006	0.65
AxD	1.78 - 0.0001 * age	0	0.025	< 0.05
Parameter	**Region 4 MCI equation**	**r^2**	**ω^2**	**p-value**
FA	0.75 – 0.0015 * age	0	0.008	0.15
MD	0.78 + 0.002 * age	0	-0.007	0.92
RD	0.39 + 0.002 * age	0	-0.004	0.51
AxD	1.68 + 0.0014 * age	0	0.008	0.15
Parameter	**Region 5 MCI equation**	**r^2**	**ω^2**	**p-value**
FA	0.78 – 0.0004 * age	0	-0.007	0.86
MD	0.72 + 0.001 * age	0.007	0.001	0.29
RD	0.31 + 0.0008 * age	0	0.006	0.18
AxD	1.56 + 0.0017 * age	0	-0.005	0.6